Two-Stage Melting of Au−Pd Nanoparticles

Sergio J. Mejía-Rosales, Carlos Fernández-Navarro, and Eduardo Pérez-Tijerina

Facultad de Ciencias Físico-Matemáticas, Universidad Autónoma de Nuevo León, San Nicolás de los Garza, Nuevo León, México 66450

Juan Martín Montejano-Carrizales

Instituto de Física, Universidad Autónoma de San Luis Potosí, San Luis Potosí, S.L.P., México 78000

Miguel José-Yacamán*

Chemical Engineering Department and Texas Advanced Materials Center, The University of Texas at Austin, Austin, Texas 78712.

Received: March 9, 2006; In Final Form: April 26, 2006

Several series of molecular dynamics runs were performed to simulate the melting transition of bimetallic cuboctahedral nanoparticles of gold−palladium at different relative concentrations to study their structural properties before, in, and after the transition. The simulations were made in the canonical ensemble, each series covering a range of temperatures from 300 to 980 K, using the Rafii−Tabar version of the Sutton and Chen interatomic potential for metallic alloys. We found that the melting transition temperature has a strong dependence on the relative concentrations of the atomic species. We also found that, previous to the melting transition, the outer layer of the nanoparticle gets disordered in what can be thought as a premelting stage, where Au atoms near the surface migrate to the surface and remain there after the particle melts as a whole. The melting of the surface below T_m is consistent with studies of the interaction of a TEM electron beam with Au and Au−Pd nanoparticles.

1. Introduction

Nanoparticles are good catalysts because of their higher number of surface atoms in comparison to bulk materials. In particular, there is a growing interest in transition metal alloys as catalysts, mainly because these materials show a considerable improvement in efficiency when compared to pure metals.[1] The study of bimetallic nanoparticles is particularly important, because the variation of size and local concentration of each atomic species offer a wide spectrum of possibilities. Au−Pd nanoparticles are among the most interesting bimetallic alloys. It has been proven, for instance, that these nanoparticles are excelent catalysts of trichloroethene (TCE), achieving a higher activity than both pure palladium nanoparticles and catalysts based on bulk palladium; this makes Au−Pd nanoparticles extremely effective agents for the remediation of various inorganic and organic groundwater contaminants.[2] More recently, Au−Pd alloys have been found to be outsanding catalysts for the hydrogenation of naphthalene and toluene,[3] which makes them important for the improvement of diesel fuels. There is also interest in the development of Au−Pd catalysts for the oxidation of alcohols to aldehydes.[4] Because the chemical activity is strongly determined both by the size and by the Au/Pd ratio at the surface,[5] stabilization of the structure and diffusion of the species into the nanoparticle become important issues to be considered.

The use of atomistic simulations is a convenient approach to study the structural and dynamical properties of metallic nanoparticles. Earlier molecular dynamics (MD) simulations of spherical gold nanoparticles[6] show that the outer atomic layers of the particle melt before the bulk and that there is hysteresis in the melting−freezing cycle. Cleveland et al. found, also by the use of MD, that truncated octahedra of Au_{459} and decahedra of Au_{146} undergo a structural transition to icosahedra before melting takes place.[7] In another MD study,[8] the premelting of the Au surface is confirmed, and it is found that the melting temperature of the Au nanoparticles strongly depends on the size of the cluster. Experimental measurements using nanocalorimetry techniques give evidence of a similar surface premelting in tin[9,10] and lead clusters.[11]

In comparison to the number of simulation studies devoted to monometallic nanoparticles, there exists only a small amount of MD simulations for bimetallic systems. Chui and Chan, using an MD algorithm to simulate Pt nanoparticles modeled by the Sutton−Chen interatomic potential, found that for $T < 300$ K, the atomic packing is fcc in the core of the particles and hcp near the surface.[12] MD simulations of Pd−Pt nanoparticles show that Pd diffuses to the surface as the system is heated;[13] a similar diffusion of Al atoms is found in MD simulations of Ni−Al nanoparticles.[14] Another MD work on bimetallic Cu−Ni nanoclusters shows that in Ni−Cu particles, the Ni core melts after the Cu surface melting occurs.[13]

In this work, we study the structure details and dynamic behavior of Au−Pd nanoparticles for the specific case of cuboctahedral geometry. We focus on several issues, such as the segregation mechanisms of the atomic species at different temperatures, the local composition, and the details of the melting transition. We performed atomistic simulations for five different stoichiometric alloy concentrations, including the cases of pure Au and pure Pd for comparison purposes, using the MD technique in the canonical ensemble.

The paper is organized as follows. The second section discusses the electron microscopy characterization of the bimetallic nanoparticles and the structure of the model used in

* To whom correspondence should be addressed. E-mail: yacaman@che.utexas.edu.

10.1021/jp0614704 CCC: $33.50
Published on Web 06/15/2006

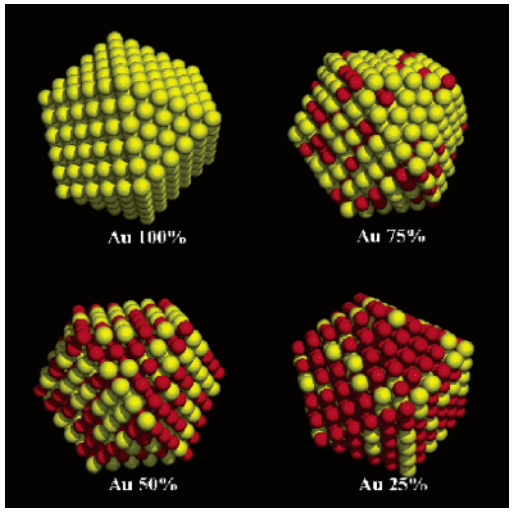

Figure 1. Initial configurations of the simulated particles. (a) Au_{100}, (b) $Au_{75}Pd_{25}$, (c) $Au_{50}Pd_{50}$, (c)$Au_{25}Pd_{75}$. The yellow spheres represent Au atoms, whereas the red spheres represent Pd atoms. The atomic identities were chosen randomly.

the simulations. Section 3 describes the atomistic simulation technique and the interatomic potentials used for this work. Results and analysis of the results are exposed in a fourth section. A discussion on the experimental context is made in the fifth section. Some concluding remarks and a summary are included in the last section.

2. Structure of the Nanoparticles

Nucleation of metallic alloys into platonic polyhedral nanoparticles has been largely documented by TEM and HRTEM images elsewhere.[15,16] We have found that, in the size range that we used in our simulations, the most commonly observed geometries corresponded to the cuboctahedral shape and to the 5-fold shapes (decahedral and icosahedral); in this paper, we will only discuss the first case.

The structure of the simulated cuboctahedral particle used as the initial configuration in the simulation series was built from a fcc with a central site, truncated in the (111) direction. The resulting structure is a cuboctahedron of 561 atoms, arranged in five shells surrounding the central atom. At the surface, 96 sites are localized in the square faces (S), 48 at the triangular faces (T), 96 at the edges (E), and 12 at the vertexes (V) of the structure.[17] Different experiments indicate that the concentration profile of the atomic species in a bimetallic nanoparticle depends strongly both on the synthesis technique and on the thermodynamic conditions at which the particles were formed;[18,19] in this MD study, the Au and Pd atoms were distributed randomly on the cuboctahedron at five different concentrations: $Au_{100\%}$, $Au_{75\%}-Pd_{25\%}$, $Au_{50\%}-Pd_{50\%}$, $Au_{25\%}-Pd_{75\%}$, and $Pd_{100\%}$. Figure 1 shows a representation of the initial configurations of the nanoparticles.

3. Simulation Conditions

The MD simulations were performed in the canonical ensemble (NVT), using the technique created by Nosé and Hoover for the control of temperature. The Nosé−Hoover thermostat works through the definition of an additional coordinate in the extended Hamiltonian, which takes charge of the dynamic scaling of the atomic velocities.[20] The integration of the equations of motion was done with the velocity Verlet algorithm, storing the velocities and forces acting on the atoms at every Δt interval.[21] The DL_POLY v2.14[22] simulation package, developed at Daresbury Laboratory, was used to perform the MD calculations. To determine the appropriate value of Δt, we performed a series of preliminary runs at different time steps, monitoring the stability of the Hamiltonian; we found that the better compromise between Hamiltonian conservation and optimization of computer time was obtained using a Δt of 1.4 fs. At each run, prior to the collection of data and statistical information, we allowed a simulation period of 140 ps, for purposes of stabilization of the unrelaxed structures. In total, each simulation run was 0.7 ns long.

It is widely recognized that the use of pair potentials is not sufficient to model the interactions of metals, mainly because pair potentials fail to reproduce the elastic properties and the surface relaxations in metallic solids. Among the different alternatives developed to deal with these technical deficiencies, the most successful empirical schemes include the embedded atom model (EAM),[23] the glue model potential,[24,25] and the Rafii−Tabar and Sutton extension of the Sutton−Chen (SC) potential.[26] The common feature of these models is the inclusion of a two-body repulsive interaction term and a many-body, long range contribution due to the local-electron density at the vicinity of each atom. The interatomic potential used in our simulations is due to Rafii−Tabar and Sutton, in a version of the Sutton and Chen potential, generalized for the case of fcc alloys. Results of simulations of fcc metals using SC potentials have reproduced fairly well surface energies and stresses,[27] and SC potentials have been used to perform MD simulations of Au−Cu[28] and Pt−Co[29] nanoparticles. In this model, the SC total energy of the system is given by

$$U(r) = \epsilon\left[\frac{1}{2}\sum_{j\neq i}\left(\frac{a}{r_{ij}}\right)^n - C\sqrt{\rho_i}\right] \quad (1)$$

where the first term accounts for the interaction between pairs of atoms separated a distance r_{ij}; in the second term, ρ_i is defined as

$$\rho_i = \sum_{j\neq i}\left(\frac{a}{r_{ij}}\right)^m \quad (2)$$

which represents a measure of the electronic local density at the ith site. The functional form of this term comes from the second moment approximation of the tight-binding model, where the cohesive energy of a solid varies as the square root of the coordination number.[30] The parameters ϵ, a, C, n, and m depend on the atomic species and are adjusted empirically; for the case of interactions of different species A and B of atoms, the following rules apply:[31]

$$m^{AB} = \frac{1}{2}(m^A + m^B) \quad (3)$$

$$n^{AB} = \frac{1}{2}(n^A + n^B)$$

$$a^{AB} = (a^A a^B)^{1/2}$$

$$\epsilon^{AB} = (\epsilon^A \epsilon^B)^{1/2}$$

The values of the adjusted parameters for the case of Au and Pd are reported elsewhere.[26]

For each nanoparticle, we performed a series of simulations formed by runs performed within a temperature range from 300 to 980 K, in intervals of 20 K. In every series, the initial configuration at 300 K was a perfect cuboctahedron with an interatomic distance of 2.88 Å; for the rest of the temperatures,

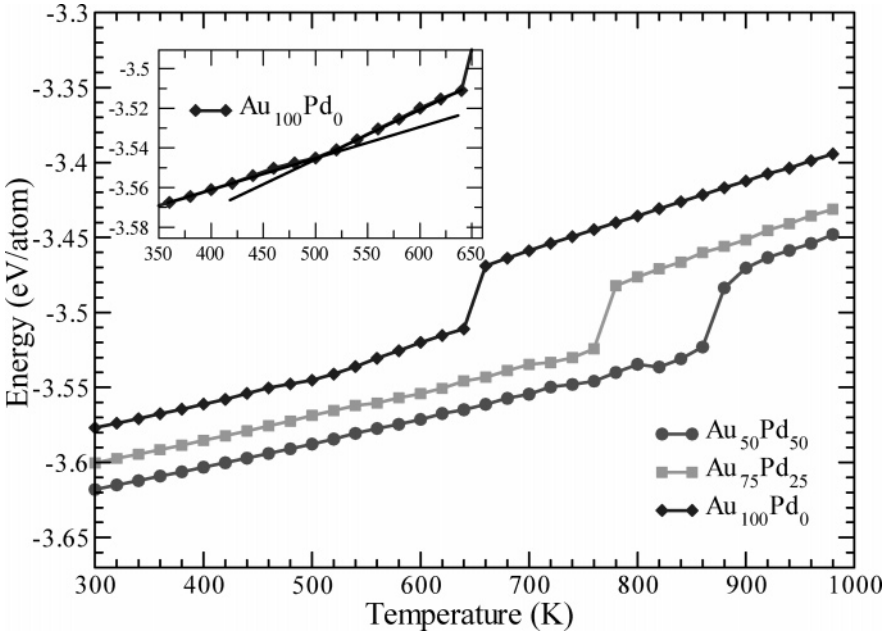

Figure 2. Temperature dependence of the configurational energy per atom for the nanoparticles during heating stage. The discontinuity in the caloric curves correspond to the melting transitions. (Inset) Change of slope in the energy curve of the Au_{100} particle below the melting transition. The slight drop of the $Au_{75}Au_{25}$ and $Au_{50}Au_{50}$ curves just before melting are due to the reorganization of the particles to more energetically favorable structures.

we used as initial configurations the final states of the particle at the immediate lower temperature, with the appropriate scaling of the atomic velocities to match the corresponding value of T.

4. Results

To investigate the thermal characteristics of the systems, the behavior of the average configuration energy per atom was monitored at the different values of temperature. The resulting caloric curves in the heating series are shown in Figure 2, for the cases of the particles with relative concentrations Au_{100}-Pd_0, $Au_{75}Pd_{25}$, and Au_{50} Pd_{50}. The melting temperature T_m in each case is located at the values of T where there is a strong change in the slope of the curves, the change in energy due to the latent heat of melting; in the figure, the strong dependence of the melting transition on the relative concentration of the species can be easily noted. The cases of $Au_{25}Pd_{75}$ and Au_0-Pd_{100} are not included in the graph because the high concentration of palladium shifted the values of T_m out of the range of temperatures studied, and the curves did not show any particular feature other than a linear increase. This dependence of T_m on the cluster alloy concentration differs from results for Au−Cu nanoparticles reported elsewhere,[28] where the two atomic species forming the alloy have very similar melting points in the bulk. Sambles[32] predicts a higher melting temperature than the one observed in our simulations for a pure gold particle of this size; following Sambles theory, the melting temperature that we found would correspond to a particle one layer smaller than the one we simulated, which can be explained if we consider that the outer layer that forms the surface of the particle melts below T_m, as is discussed below. We can also note that, for the case of the $Au_{50}Pd_{50}$ particle, previous to the melting transition, the configurational energy drops down slightly due to a geometrical reorganization of the particle to a more energetically favorable structure, as could be noted by the detailed frame-by-frame analysis of the evolution of the structure; a similar behavior was obtained at higher concentrations of palladium. For the $Au_{100}Pd_0$ particle in our simulations, the value of the critical temperature T_m is smaller than those obtained by Chushak and Bartell for 459-atom particles[33] and by Nam et al. for a 561-atom particle.[34] This discrepancy may be explained by the differences in the models for the atomic interactions but also by the fact that, in both references, the temperature was kept constant, merely forcing the rescaling of the velocities, without the use of a thermostat in the Hamiltonian. The use of a Nosé thermostat allows the simulation of the system as it evolves in the phase space, following the statistics of a canonical ensemble, whereas the method of forcing the rescaling of velocities to keep the kinetic energy constant is unphysical and may lead to the violation of energy partition.[35]

Figure 3 shows the final configurations of the particles before and after the melting transition, along with their corresponding diffraction patterns. The simulated diffraction patterns were made using the SimulaTEM package.[36] We can recall, in the first place, the melting of the surface below T_m and, in second place, that segregation of Au to the surface has occurred before melting in the alloy nanoparticles; this is particularly relevant for catalysis, because the degree of catalytic activity of the particle depends on the relative concentrations of Pd and Au on the surface.

Prior to the melting transition, the slopes of the energy curves change slightly, which can be interpreted as changes in the structure of the particles. In the inset of Figure 2, it can be noted that this change occurs around $T = 500$ K for the case of the $Au_{100}Pd_0$ particle, whereas a similar change of slope occurs at 560 K for the $Au_{75}Pd_{25}$ particle and at 700 K for the $Au_{50}Pd_{50}$ particle. The self-diffusion coefficients for the two atomic species were calculated from the slope of the mean-square displacement $r^2(t)$, following the Einstein equation

$$D = \frac{\langle r^2(t) \rangle}{6t} \tag{4}$$

In the diffusion coefficient curves for the gold and palladium, shown in Figure 4, it is more clearly noted that at least some of the atoms of both species start to migrate from their original lattice sites at these temperatures.

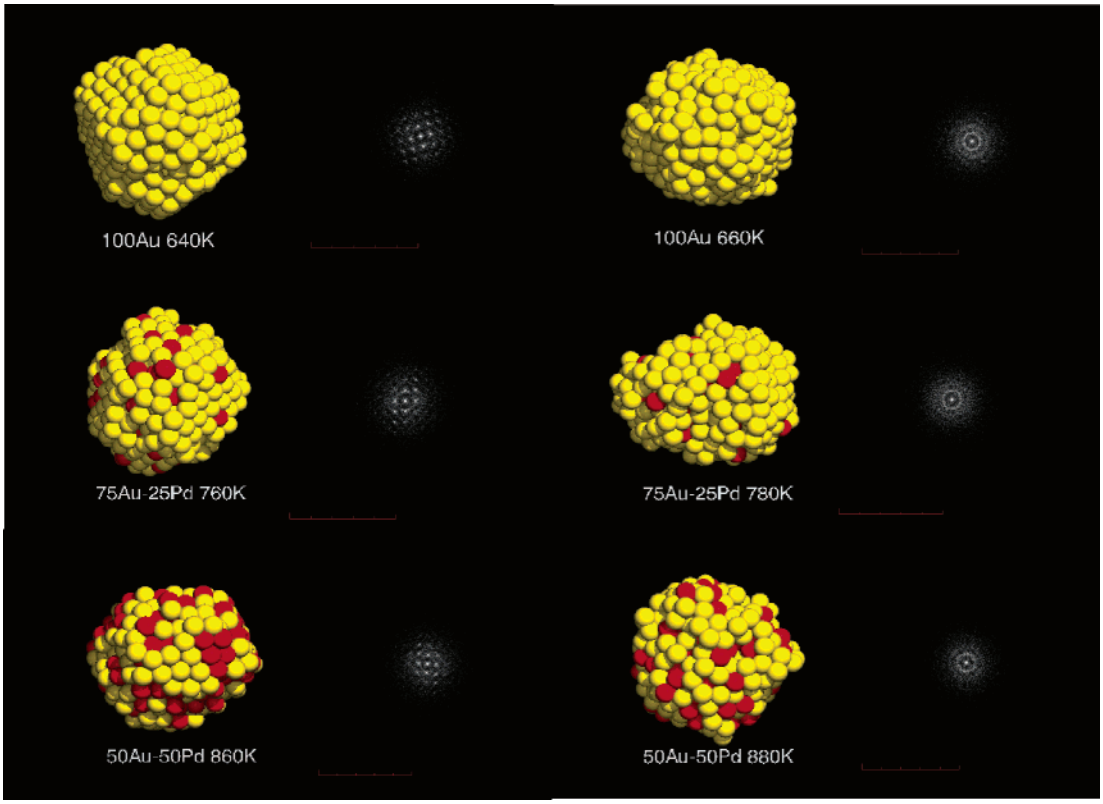

Figure 3. Final configurations of the nanoparticles before (left) and after (right) the melting transition, along with the corresponding diffraction patterns.

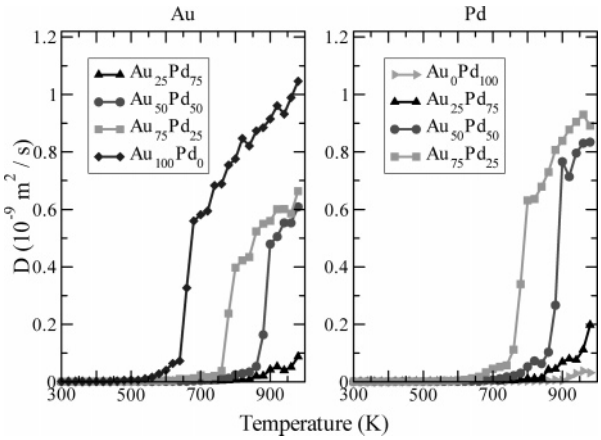

Figure 4. Diffusion coefficients for the different simulated nanoparticles during the heating stages. Left: Gold; right: Palladium. Note the increase in the diffusion for both species even before the melting transition.

A more detailed analysis of the change in the structure of the particles was done monitoring the concentration of atoms at a distance *r*, measured from the center of the particle. Results from this analysis are shown in Figure 5, where lighter regions correspond to higher atomic concentrations, and darker regions represent low or nule presence of atoms. From the figure, it can be noted that, as expected, at low values of *T*, the atoms are distributed in the particle as a set of shells, each shell corresponding to one *equivalent site* in the geometry of the structure. For a 561-atom cuboctahedron like the one used in our simulations, there exist 23 different equivalent sites forming 5 cuboctahedral layers of atoms, and most of these equivalent sites are well differentiated in different *shells* at low temperatures before melting takes place. We can also observe that the shells that define the outer layer melt before the core of the particle,

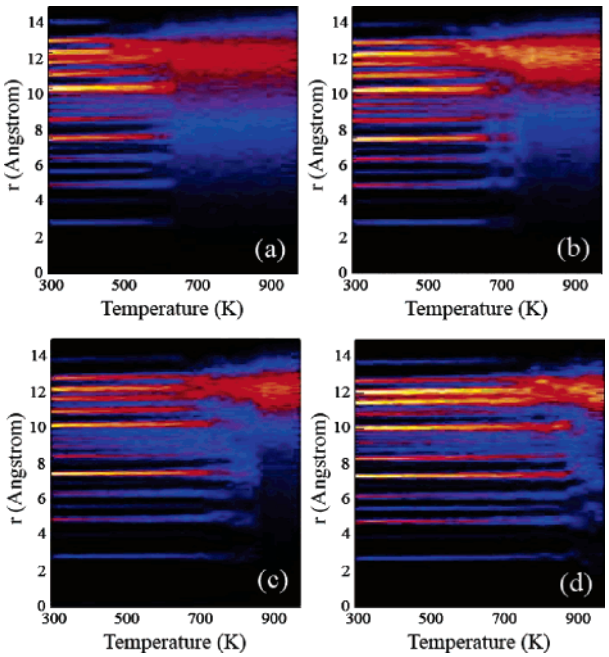

Figure 5. Temperature dependence of the density profile of atoms with respect to the distance, in Å, from the atom to the center of the nanoparticle. At low temperature, the particle shows a well-defined set of layers, corresponding to the layers of high intensity in the plots; once the particle melts, the layers arrangement dissappears. The external shells melt first; core layers melt simultaneously at a higher temperature than the external shell. (a) Au_{100}, (b) $Au_{75}Pd_{25}$, (c) $Au_{50}Pd_{50}$, (d) $Au_{25}Pd_{75}$.

in accordance with the measurements of the diffusion coefficient. The coexistence of a crystal core with a melted surface at the vicinity of T_m has been reported previously in simulations of particles of similar size, and it has been described trough several

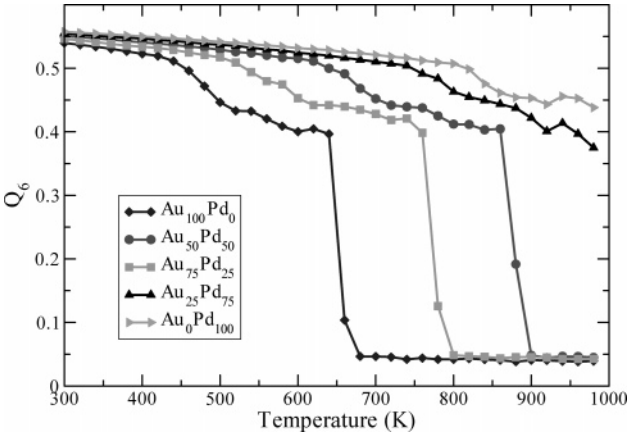

Figure 6. Temperature dependence of the global order parameter Q_6 on the heating series.

models that take into account the solid−liquid interfacial tension.[32,37,38]

The atomic arrangement can be described quantitatively through the order parameter Q_6:[39]

$$Q_6 = \left(\frac{4\pi}{13}\sum_{m=-6}^{6}\left|Q_{6m}\right|^2\right)^{1/2} \tag{5}$$

$$Q_{6m} = \frac{\sum_{i=1}^{N} N_n(i) q_{6m}(i)}{\sum_{i=1}^{N} N_n(i)} \tag{6}$$

where N is the total number of atoms in the particle, $N_n(i)$ is the number of first neighbors for the ith atom, and $q_{6m}(i)$ measures the local order around the ith atom considering the average of the spherical harmonics Y_{6m} of the bonds with the $N_n(i)$ neighbors:

$$q_{6m}(i) = \frac{\sum_{j=1}^{N_n(i)} Y_{6m}(\mathbf{r}_{ij})}{N_n(i)} \tag{7}$$

Defined in this way, the order parameter Q_6 becomes a fair criteria to identify the resulting structures of the heating process, because a specific structure is characterized by well-defined value of Q_6: a perfect FCC structure gives a value $Q_{6FCC} = 0.575$, whereas an icosahedron gives $Q_{6Ih} = 0.663$, for example.[33] In accordance with this, our original cuboctahedral Au_{100} structure, relaxed at 300 K, gave a value of $Q_6 = 0.540$. However, at higher temperatures, any of these structures will give values of the order parameter smaller than in the perfect array, and, for melted states, the value of Q_6 will drop down to values close to zero.

To identify the features of the melting transition, we show in Figure 6the values of Q_6 as function of the temperature during the heating series. In this graph, it can be clearly noted that before the particle core melts, there is a rearrangment of the particle that lowers the value of the order parameter below that characteristic of a FCC structure. We can see in the images in Figure 3 that, immediatly before melting, the particles still resemble the original cuboctahedra, but the atoms at the surface are disordered to a degree that explains the drop of the bond order parameter. This observation is consistent with the measurements of the fall of the local order parameter q_6 at the surface of the particle, around 100 K before the particle melts as a whole. This behavior somewhat differs from the results from Wang et al., who found that the surface does not melt before the bulk melting temperature in pure gold icosahedra but only gets softened by the increase of mobility of vertex and edge atoms.[40] This surface phenomena has relevance from the practical point of view; indeed, the atomic rearrangements at the surface before the melting of the particle may have important consequences in the chemical activity of the particle.

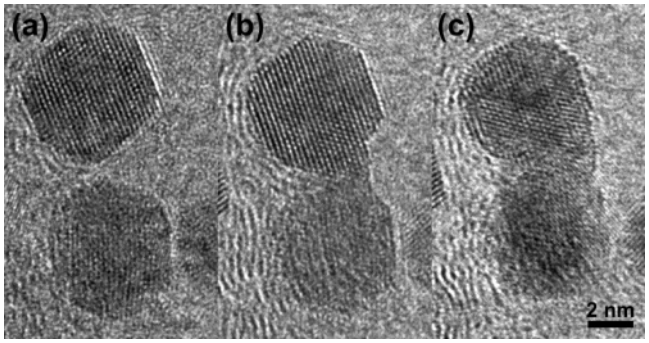

Figure 7. Coalescence of two Au particles are induced by the TEM electron beam. (a) Particles before contact. (b) As the particles start to interact, the temperature of the particle raises close to but below T_m, and as a result, (c) the layer of atoms at the surface becomes disordered.

5. Discussion

Several interesting points arise from our calculations that have important implications from both theoretical and practical points of view. First, it is important to note that there is indeed a sharp (first order) transition on the bimetallic nanoparticles, which corresponds to a true melting point. The melting point can be identified with precision by a very sharp loss of coherence on the diffraction pattern (FFT), as is shown in Figure 3. This decoherence justifies from the theoretical perspective the classical experiment of Borel and Buttet,[41] which measured T_m by the analysis of diffraction patterns. Another relevant result is that the critical melting temperature T_m strongly depends on the relative concentration of the metals. However, and despite the sharp transition at T_m, there is a premelting stage at which the surface atoms increase their mobility, as shown in Figure 5. This premelting is even more transparent by examination of the orientational order parameter of Figure 6: In the case of 100% Au particles, there is a plateau region in the order parameter at the range of 520− 660 K and then a sharp fall at 675 K; this plateau will correspond to a premelting state with a sharp surface dissorder. On the other hand, the presence of a second metal does increase both the value of T_m and the plateau range. For instance, a particle with a 50/50 proportion of Au/Pd will gain 200 K in T_m, and the plateau will be extended to the range 720−860 K, which will be a determining factor in the catalytic properties of the particle.

The theoretical prediction of surface premelting is consistent with previous reports for pure gold.[42,7] However, the most interesting implication is that we should be able to see a direct premelting of the surface when the particle is heated. This is indeed shown experimentally in Figure 7, where two particles are induced to coalesce by the TEM e-beam. Then, according to Lehtinen and Zachariah,[43] the reaction is exotermic and the temperature increases. This induces that the local temperature of the particle rapidly raises to near the T_m. As can be seen, a layer of atoms becomes first mobile on the surface, in accordance with the results of the MD simulations.

6. Conclusions

The empirical Rafii−Tabar and Sutton version of the Sutton−Chen interatomic potential was used to simulate the dynamics of Au−Pd bimetallic nanoparticles, through several series of MD runs in the canonical ensemble. Based on TEM observations, the initial geometry was a 561-atom cuboctahedron, with concentrations $Au_{100\%}Pd_{0\%}$, $Au_{75\%}Pd_{25\%}$, $Au_{50\%}Pd_{50\%}$, $Au_{25\%}Pd_{75\%}$, and $Au_{0\%}Pd_{100\%}$. The particles were heated above the melting point. Previous to the melting of the core of the particle, the shells that define the outer layer melt at a lower temperature, and this two-stage melting transition is more evident at higher concentrations of Au. This premelting of the surface is in accordance with Cs-corrected TEM observations. After melting of the outer shell, gold atoms migrate to the surface; this rearrangement may be of particular relevance in the chemical activity of the particle, and it deserves to be taken into consideration for the design of synthesis processes of alloy nanoparticles.

Acknowledgment. This work was supported by the International Center for Nanotechnology and Advanced Materials of The University of Texas at Austin (ICNAM), the Council for Science and Technology of the State of Nuevo León, México, and the National Council for Science and Technology, México (CONACYT), Grant 43772. Computing time on the IBM Power4 resource at the Texas Advanced Computing Center, The University of Texas at Austin, is also acknowledged. We thank the Welch Foundation for financial support.

References and Notes

(1) Liu, H. B.; Pal, U.; Medina, A.; Maldonado, C.; Ascencio, J. A. *Phys. Rev. B: Condens. Matter Mater. Phys.* **2005**, *71*.
(2) Nutt, M. O.; Hughes, J. B.; Wong, M. S. *Environ. Sci. Technol.* **2005**, *39*, 1346−1353.
(3) Pawelec, B.; Cano-Serrano, E.; Campos-Martin, J. M.; R. M. Navarro, S. T.; Fierro, J. L. G. *Appl. Catal., A* **2004**, *275*, 127−139.
(4) Enache, D. I.; Edwards, J. K.; Landon, P.; Solsona-Espriu, B.; Carley, A. F.; Herzing, A. A.; Watanabe, M.; Kiely, C. J.; Knight, D. W.; Hutchings, G. J. *Science* **2006**, *311*, 362−365.
(5) Hermans, S.; Devillers, M. *Catal. Lett.* **2001**, *99*, 55−64.
(6) Lewis, L. J.; Jensen, P.; Barrat, J.-L. *Phys. Rev. B: Condens. Matter Mater. Phys.* **1997**, *56*, 2248−2257.
(7) Cleveland, C. L.; Luedtke, W. D.; Landman, U. *Phys. Rev. Lett.* **1998**, *81*, 2036−2039.
(8) Shim, J.-H.; Lee, B.-J.; Cho, Y. W. *Surf. Sci.* **2002**, *512*, 262−268.
(9) Lai, S. L.; Guo, J. Y.; Petrova, V.; Ramanath, G.; Allen, L. H. *Phys. Rev. Lett.* **1996**, *77*, 99−102.
(10) Bachels, T.; Güntherodt, H.-J. *Phys. Rev. Lett.* **2000**, *85*, 1250−1253.
(11) Kofman, R.; Cheyssac, P.; Lereah, Y.; Stella, A. *Eur. Phys. J. D* **1999**, *9*, 441−444.
(12) Chui, Y. H.; Chan, K. Y. *Phys. Chem. Chem. Phys.* **2003**, *5*, 2869−2874.
(13) Sankaranarayanan, S. K. R. S.; Bhethanabotla, V. R.; Joseph, B. *Phys. Rev. B: Condens. Matter Mater. Phys.* **2005**, *71*, 195415(15).
(14) Chushak, Y. G.; Bartell, L. S. *J. Phys. Chem. B* **2003**, *107*, 3747−3751.
(15) Yacamán, M. J.; Ascencio, J. A.; Liu, H. B.; Gardea-Torresdey, J. *J. Vac. Sci. Technol. B* **2001**, *19*, 1091−1103.
(16) Buffat, P.-A.; Flüeli, M.; Spycher, R.; Stadelmann, P.; Borel, J.-P. *Faraday Discuss.* **1991**, *92*, 173−187.
(17) Montejano-Carrizales, J. M.; Rodríguez-López, J. L.; Gutierrez-Wing, C.; Miki-Yoshida, M.; José-Yacamán, M. J. *Encyclopedia of Nanoscience and Nanotechnology*; American Scientific Publishers: Stevenson Ranch, 2004; Vol. 2.
(18) Reifsnyder, S. N.; Lamb, H. H. *J. Phys. Chem. B* **1999**, *103*, 321−329.
(19) Lee, A. F.; Baddeley, C. J.; Hardacre, C.; Ormerod, R. M.; Lambert, R. M. *J. Phys. Chem.* **1995**, *99*, 6096−6102.
(20) Nosé, S. *J. Chem. Phys.* **1984**, *81*, 511.
(21) Allen, M. P.; Tildesley, D. J. *Computer Simulation of Liquids;* Oxford Science Publications: New York, 2004; p 1987.
(22) Smith, W.; Forester, T. R. *DL_POLY Package of Molecular Simulation Subroutines*; 1996.
(23) Foiles, S. M.; Baskes, M. I.; Daw, M. S. *Phys. Rev. B: Condens. Matter Mater. Phys.* **1986**, *33*, 7983−7991.
(24) Ercolessi, F.; Parrinello, M.; Tosatti, E. *Surf. Sci.* **1986**, *177*, 314−328.
(25) Gulseren, O.; Ercolessi, F.; Tosatti, E. *Phys. Rev. Lett.* **1998**, *80*, 3775−3778.
(26) Rafii-Tabar, H.; Sutton, A. P. *Philos. Mag. Lett.* **1991**, *63*, 217−224.
(27) Todd, B. D.; Lynden-Bell, R. M. *Surf. Sci.* **1993**, *281*, 191−206.
(28) Rodríguez-López, J. L.; Montejano-Carrizales, J. M.; Yacamán, M. J. *Appl. Surf. Sci.* **2003**, *219*, 56−63.
(29) Chui, Y. H.; Chan, K.-Y. *Mol. Sim.* **2004**, *30*, 679−690.
(30) Leach, A. *Molecular Modeling: Principles and Applications*, 2nd ed.; Prentice Hall: New York, 2001.
(31) Rafii-Tabar, H. *Phys. Rep.* **2000**, *325*, 239−310.
(32) Sambles, J. R. *Proc. R. Soc. London, Ser. A* **1971**, *324*, 339−351.
(33) Chushak, Y. G.; Bartell, L. S. *J. Phys. Chem. B* **2001**, *105*, 11605−11614.
(34) Nam, H. S.; Hwang, N. M.; Yu, B. D.; Yoon, J. K. *Phys. Rev. Lett.* **2002**, *89*.
(35) Harvey, S. C.; Tan, R. K.-Z.; Cheatham, T. E., III *J. Comp. Chem.* **1998**, *19*, 726−740.
(36) Beltrán del Rio, L. *SimulaTEM 1.1*; Mexico: UNAM; 1998.
(37) Reiss, H. W. *I. B. J. Colloid Sci.* **1948**, *3*, 551.
(38) Hanszen, K. J. *Z. Phys.* **1960**, *157*, 523.
(39) Chushak, Y.; Bartell, L. S. *J. Phys. Chem. A* **2000**, *104*, 9328−9336.
(40) Wang, Y.; Teitel, S.; Dellago, C. *Chem. Phys.* **2005**, *122*,.
(41) Borel, J.-P. *Surf. Sci.* **1981**, *106*, 1−9.
(42) Ercolessi, F.; Andreoni, W.; Tosatti, E. *Phys. Rev. Lett.* **1991**, *66*, 911−914.
(43) Lehtinen, K. E. J.; Zachariah, M. R. *Phys. Rev. B* **2001**, *63*, 205402−1.